4646 *Macromolecules* **2009**, *42*, 4646–4650
DOI: 10.1021/ma802457v

Macromolecules
ARTICLE

Nanomorphology of Bulk Heterojunction Organic Solar Cells in 2D and 3D Correlated to Photovoltaic Performance

Sophie Barrau,[†,‡] Viktor Andersson,[†,‡] Fengling Zhang,*[,†,‡] Sergej Masich,[§] Johan Bijleveld,[⊥] Mats R. Andersson,[⊥] and Olle Inganas[†,‡]

[†]*Biomolecular and Organic Electronics, Department of Physics, Chemistry and Biology, Linkoping University, SE-58183 Linkoping, Sweden,* [‡]*Center of Organic Electronics (COE), Linkoping University, SE-58183 Linkoping, Sweden,* [§]*Department of Cell and Molecular Biology, Karolinska Institutet, 171 77 Stockholm, Sweden, and* [⊥]*Polymer Chemistry, Department of Chemical and Biological Engineering/Polymer Technology, Chalmers University of Technology, SE-412 96 Gothenburg, Sweden*

Received November 3, 2008; Revised Manuscript Received May 15, 2009

ABSTRACT: Control of the nanoscale morphology of the donor−acceptor material blends in organic solar cells is critical for optimizing the photovoltaic performances. The influence of intrinsic (acceptor materials) and extrinsic (donor:acceptor weight ratio, substrate, solvent) parameters was investigated, by atomic force microscopy (AFM) and electron tomography (ET), on the nanoscale phase separation of blends of a low-band-gap alternating polyfluorene copolymers (APFO-Green9) with [6,6]-phenyl-C_{71}-butyric acid methyl ester ([70]PCBM). The photovoltaic performances display an optimal efficiency for the device elaborated with a 1:3 APFO-Green polymer:[70]PCBM weight ratio and spin-coated from chloroform solution. The associated active layer morphology presents small phase-separated domains which is a good balance between a large interfacial donor−acceptor area and continuous paths of the donor and acceptor phases to the electrodes.

1. Introduction

Organic semiconducting materials open the way of low-cost, flexible, and large-scale solar cells. Recently, efficiencies above 5% and to 6.1% have been reported for bulk-heterojunction cells[1−3] characterized by an interpenetrating network of donor and acceptor materials. Classically, the electron donor material (D) is a semiconducting polymer and the electron acceptor material (A) a [6,6]-phenyl-C_{61}-butyric acid methyl ester (PCBM).[4−6] The energy conversion mechanism of organic solar cells involves light absorption and exciton generation, exciton diffusion, exciton dissociation with charge generation, charge transport, and charge collection. A domain size commensurate with the exciton diffusion length ($<5-10$ nm) is required, and a large interfacial D−A area is necessary for an efficient exciton dissociation.[7] However, at the same time it is important to have continuous paths through both the D and A phases for efficient transport between electrodes. A too intimate mixing can limit the charge carrier transport properties.[8] A lot of effort has been done in improving the properties of organic photovoltaic devices by the control of the morphology of the active layer.[9−13] The morphology depends on properties inherent to the polymer and the fullerene, such as fundamental interaction parameters between the two components (relative miscibility), and on external influences associated with device fabrication, such as solvent choice (solvent evaporation rate), overall concentration of the blend components, deposition technique, and thermal and/or solvent annealing. The optimization of these parameters allows creating the nanoscale phase-separated domains which give the maximal photovoltaic performances. Power conversion efficiency (PCE) is dependent on both the photocurrent and the photovoltage of the diode under illumination. The short-circuit current (J_{sc}) is sensitive to the absorption coefficient and the morphology of the active layer[14−16] while the open-circuit voltage (V_{oc}) depends on the energy difference between the LUMO (lowest unoccupied molecular orbital) of the acceptor and the HOMO (highest occupied molecular orbital) of the donor. To achieve high photocurrent and/or high photovoltage, low-band-gap ($E_g < 2$ eV) polymers and alternating polyfluorene copolymers (APFO-Greens) have been synthesized with absorption ranges that match solar irradiance in order to harvest photons at long wavelength.[17,18] A $J_{sc} \sim 9$ mA/cm^2 was achieved in the solar cells based on APFO-Green5,[19] and a V_{oc} larger than 0.8 V was reported for APFO-Green9. A study of the opto-electronic properties of this APFO-Green9 polymer has already been reported,[20] displaying a decent J_{sc} (6.5 mA/cm^2), an impressive V_{oc} (0.81 V), and a PCE of 2.3% by combining the polymer with [70]PCBM. [70]PCBM was used to replace [60]PCBM as electron acceptor to harvest the photons in the region around 500 nm and thereby to compensate the valley in the absorbance of APFO-Green9, allowing an enhancement of photocurrent.

In this paper, we focus on the morphology of APFO-Green9:[70]PCBM blends, we report the influence of parameters such as the weight ratio of the blend constituents, the substrate, the solvent, and the acceptor materials on the active layer morphology characterized by atomic force microscopy (AFM) and electron tomography (ET), and we correlate the nanoscale phase-separated domains to the photovoltaic parameters.

2. Experimental Part

Materials. An alternating polyfluorene copolymer APFO-Green9 was used as electron donor. The synthetic route for the synthesis of the polymer was described previously.[20] [6,6]-Phenyl-C_{71}-butyric acid methyl ester ([70]PCBM) from Solenne Netherlands was used as electron acceptor. The structure of the materials is shown in Figure 1a,b. For comparison, a blend with [60]PCBM (Figure 1c) was also used.

*Corresponding author. E-mail: fenzh@ifm.liu.se.

 Published on Web 06/05/2009

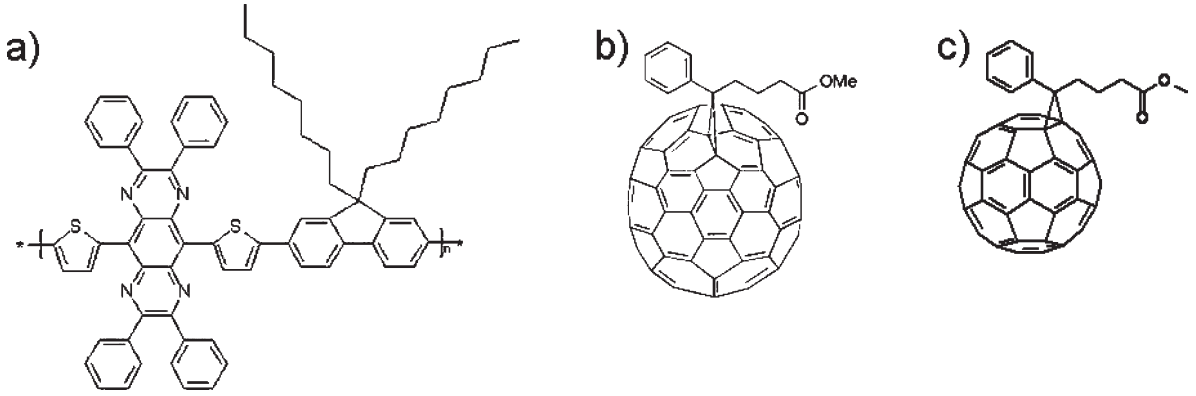

Figure 1. Structure of (a) APFO-Green9, (b) [70]PCBM, and (c) [60]PCBM.

Device Preparation. Cleaned indium tin oxide (ITO)-coated glass substrates were covered with a poly(ethylenedioxythiophene)−poly(styrenesulfonate) (PEDOT:PSS) layer by spin-coating at 2500 rpm (40 nm) and then annealing at 120 °C for 5 min to remove the residual water. The active layer of APFO-Green9 and [70]PCBM blends was spin-coated at 2000 rpm from chloroform (CF) solutions, on the top of PEDOT:PSS. The corresponding thicknesses vary from 50 to 80 nm. The blend with [60]PCBM was spin-coated at the same spin speed. From chloroform:dichlorobenzene (10:1) mixture solution or dichlorobenzene (DCB) solution, the active layer spin speeds were 2000 and 500 rpm, respectively, implying comparable thicknesses with those from chloroform. The samples were finally transferred into the vacuum chamber to deposit LiF (0.6 nm) and Al (60 nm). For the film spin-coated directly on silicon substrates, the spin speed is 1000 rpm, which identical to the one used for construction of devices.

Atomic Force Microscopy. The film surface morphology was investigated by atomic force microscopy (AFM) with a Dimension 3100 system (Digital Instruments/Veeco) operating in tapping mode. Silicon cantilevers (NSG10) with a force constant of 5.5−22.5 N/m, a resonance frequency of 190−325 kHz, and a tip curvature radius of 10 nm were used. For all the samples, the scan size is 2 μm × 2 μm.

Electron Tomography. The active layers of the solar cells were placed on copper grids. 10 nm gold particles for image alignment were applied to one surface of the film, as described earlier.[21] Image series of the tilted specimens were collected in a transmission electron microscope (FEI CM200 FEG, 200 kV), in a range of ca. −60° to 60° with 0.5° increment. A cooled slow scan 2048 × 2048 TemCam-F224 CCD and software for automated data collection (TVIPS, Gauting, Germany) were used for data recording. The TEM magnification was 20 000× and the post-magnification was 1.531×, resulting in a pixel size of 7.84 Å at the specimen level. The target underfocus during data collection was set to 2−2.5 μm, corresponding to the first contrast transfer function zero at ∼2 nm. The obtained images were used to make three-dimensional reconstructions of the samples.

Photovoltaic Device Characterization. Solar cells were characterized using white light illumination from a solar simulator AM1.5 (100 mW·cm^{-2}). The photocurrent (J_{sc}), the photovoltage (V_{oc}), the power conversion efficiency (PCE), and the fill factor (FF) were deduced from $I-V$ curves.

3. Morphology

Polymer:[70]PCBM Ratio. The influence of [70]PCBM concentration on the phase-separated domains was investigated. The morphology of a series of films spin-coated from chloroform solutions containing different weight ratios of polymer to PCBM were imaged with AFM. The topography images of APFO-Green9:[70]PCBM with ratios of 1:1, 1:2, 1:3, and 1:4 are shown in Figure 2. The 1:1 and 1:2 blends present a smooth surface with a root-mean-square (rms) roughness of 0.47 nm. From the 1:3 blend, some small phase-separated domains appear. The rms roughness is 0.54 nm. With increasing [70]PCBM content, the domains become bigger and the rms roughness is 1.08 nm. For all the ratios, the associated phase images (not shown) do not display a contrast.

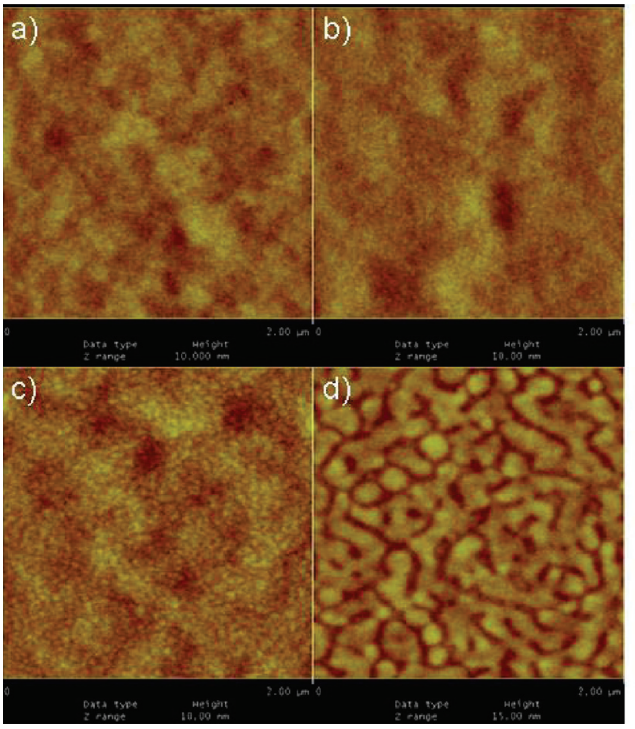

Figure 2. AFM images in topography of APFO-Green9:[70]PCBM spin-coated onto ITO/PEDOT:PSS substrate with (a) 1:1, (b) 1:2, (c) 1:3, and (d) 1:4 weight ratios. The Z range is 10 nm for (a−c) and 15 nm for (d).

For the 1:1 and 1:2 ratios, we expect a fine mixture of both materials and so a good miscibility. By increasing the PCBM content from 1:3, some phase-separated regions containing an excess of [70]PCBM appear. Hoppe et al.[7,22] obtained comparable pictures for MDMO-PPV:[60]PCBM spin-casted films from toluene solutions. The authors showed that for the highest ratios some flattened PCBM nanoclusters covered by a polymer-enriched "skin" layer can be observed. However, the study of the compositional depth profiles of APFO3:[60]PCBM 1:3 blends spin-coated from chloroform solutions displays the formation of vertical phase segregation.[23] The free surface of the film is enriched with the lower surface energy blend component polymer. The spin-coating process freezes the blend in

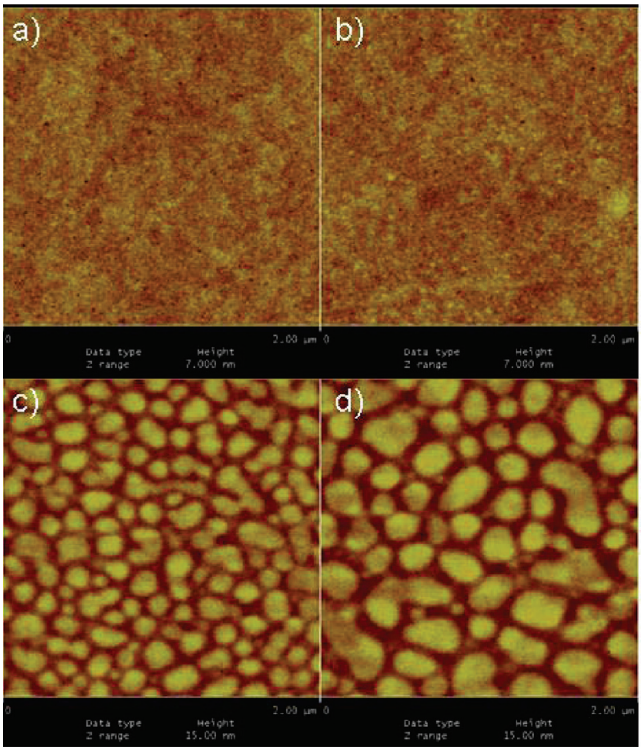

Figure 3. AFM images in topography of APFO-Green9:[70]PCBM spin-coated onto silicon substrate with (a) 1:1, (b) 1:2, (c) 1:3, and (d) 1:4 weight ratios. The *Z* range is 7 nm for (a, b) and 15 nm for (c, d).

a nonequilibrium state, implying a multilayer structure with polymer-enriched layer and PCBM-enriched layer inside the film. Recently, the study of the same APFO-Green9:[70]PCBM blend by photoelectron spectroscopy[24] displays that the interface between the PEDOT:PSS and the blend is a PCBM-enriched layer.

Substrate. Because of the specific surface energy, the nature of the substrate can modify the morphology of the active layer. To display this difference, silicon wafer were used as substrate, and the resulting active layer phase separation was compared to the one on PEDOT:PSS. The morphology of the previous blend solutions spin-coated on the silicon substrate is presented in Figure 3. The 1:1 and 1:2 blends present a very smooth surface. The rms roughness is 0.33 nm for the 1:1 blend and 0.35 nm for the 1:2 blend. Like previously, from a 1:3 ratio domains appear. However from this ratio, the size of the domains is bigger for the films onto silicon substrate. The rms roughness is 1.46 and 1.78 nm for 1:3 and 1:4 blends, respectively.

The morphology of the blends is significantly affected by the nature of the substrate, more precisely by the surface energy and the interactions between the blend constituents and the substrate. The composition of the film in the region close to the substrate is mainly affected.[25] For low concentrations of [70]PCBM, the smooth films indicate the formation of an homogeneous blend. For high concentrations, the very rough surface of the blends and the presence of big domains suggest the presence of higher repulsion forces between [70]PCBM and the silicon substrate.

Solvent. The choice of the solvent is a key point in the formation of phase-separated domains. A significant morphological difference is observed by the use of nonaromatic (chloroform) or aromatic (toluene, chlorobenzene, dichlorbenzene) solvents.[8,16,26,27] The topography images of APFO-Green9:[70]PCBM film with a 1:3 ratio and spin-coated from DCB solution and from a CF:DCB 10:1 mixture solution are

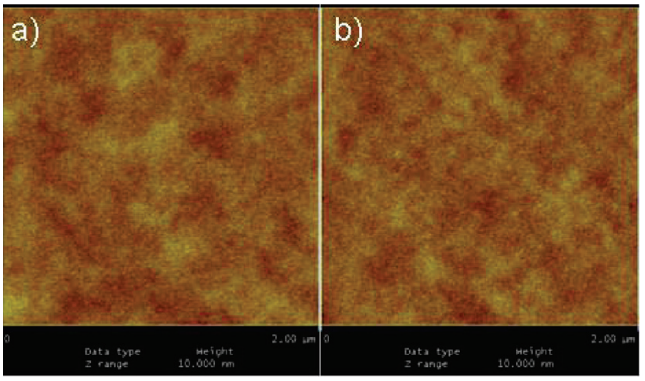

Figure 4. AFM images in topography of 1:3 APFO-Green9:[70]PCBM spin-coated from (a) CF:DCB solvent mixture and (b) DCB. The *Z* range is 10 nm.

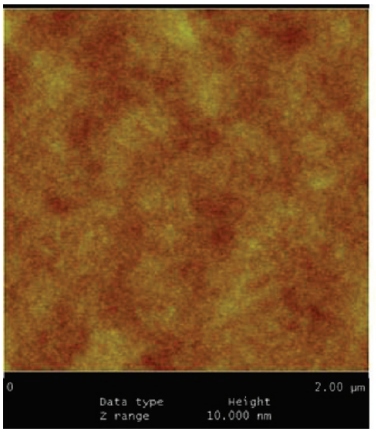

Figure 5. AFM images in topography of 1:3 APFO-Green9:[60]PCBM. The *Z* range is 10 nm.

presented Figure 4. The film elaborated from DCB presents a very smooth surface with a rms roughness of 0.36 nm while the one elaborated from the CF:DCB mixture has a rms roughness of 0.39 nm, intermediary between the roughness of the films spin-coated from CF and from DCB. The use of DCB as a solvent avoids the formation of phase-separated domains. The morphological difference can be explained by the higher solubility of the blend constituents in DCB compared to CF, resulting in the formation of smoother films. A similar behavior has already been reported for APFO3-polymer-based blend with a homogeneous composition in the vertical direction.[28] Wienk et al.[29] obtained similar active layer topography for MDMO-PPV:[70]PCBM blends spin-coated from DCB.

Acceptor. Because of the broad absorption peak, the use of [70]PCBM instead of [60]PCBM is very attractive to improve the solar cells performances. However, the change of the acceptor material has some consequences on the D−A blend morphology. The surface morphology of APFO-Green9:[60]PCBM blend with a 1:3 ratio is shown in Figure 5. The APFO-Green9:[60]PCBM film presents a smooth surface with a rms roughness of 0.36 nm, which is lower than the one obtained for the blend with [70]PCBM (Figure 2a,b) at the lowest ratio (1:1). And for the same 1:3 ratio (Figure 2c), the mixture of APFO-Green9 with [60]PCBM displays a good blend while the mixture with [70]PCBM implies a phase separation.

The tomography images of these samples are presented in Figure 6. Reconstruction overviews (Figure 6a,b) and middle sections (Figure 6c,d) of APFO-Green9:[60]PCBM (1:3) and APFO-Green9:[70]PCBM (1:3), respectively, are displayed.

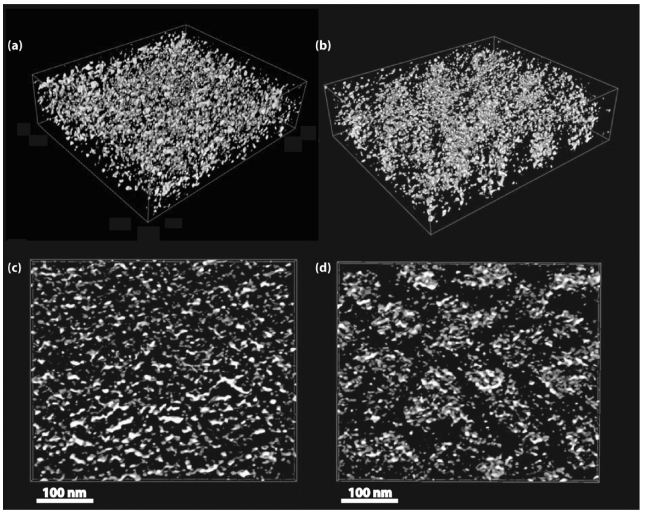

Figure 6. Electron tomography reconstructions of APFO-Green9:[60]PCBM (1:3) (a) and APFO-Green9:[70]PCBM (1:3) (b) cast on PEDOT:PSS. The reconstructions are low-pass filtered at 10 nm. (c) and (d) show planar sections (ca. 16 nm thick) from the middle of the reconstructions.

Table 1. Performance of the Diodes

active layer	solvent	J_{sc} (mA·cm^{-2})	V_{oc} (V)	FF	PCE (%)
APFO-Green9: [70]PCBM (1:1)	CF	1.9	0.81	0.34	0.52
APFO-Green9: [70]PCBM (1:2)	CF	4.5	0.84	0.36	1.3
APFO-Green9: [70]PCBM (1:3)	CF	6.1	0.84	0.42	2.2
APFO-Green9: [70]PCBM (1:4)	CF	5.3	0.82	0.44	1.9
APFO-Green9: [70]PCBM (1:3)	CF:DCB	5.7	0.8	0.39	1.8
APFO-Green9: [70]PCBM (1:3)	DCB	4.4	0.77	0.42	1.4
APFO-Green9: [60]PCBM (1:3)	CF	4.6	0.83	0.41	1.6

The reconstructions are low-pass filtered at 10 nm. The images show that when [70]PCBM is used in the blend, larger and more pillar-like structures of PCBM-rich domains are formed compared to APFO-Green9:[60]PCBM. APFO-Green9:[60]PCBM seems to have a finer and more well-dispersed morphology.

A proposed hypothesis to explain this morphological difference is the lower solubility of [70]PCBM in chloroform, resulting in the formation of PCBM domains in the films. However the nature of the acceptor material presents also an effect on the D−A interactions.[30,31] Then, the morphological difference can also be explained by the stronger repulsion of APFO-Green9 with [70]PCBM than with [60]PCBM.

4. Photovoltaic Properties

The performances of the organic solar cells are strongly correlated to the morphology of the active layer. The photovoltaic parameters such as J_{sc}, V_{oc}, PCE, and FF are reported (Table 1) for the different diodes discussed previously. The best parameters are obtained for APFO-Green9:[70]PCBM (1:3) with chloroform as a solvent. J_{sc}, V_{oc}, and PCE are maximal with values of 6.1 mA·cm^{-2}, 0.84 V, and 2.2%, respectively, and the associated FF is 0.42.

The optimal weight ratio of the two blend components is strongly dependent on the D−A material miscibility. Classically, for P3HT:PCBM blends the ratios which give the best performances are lower than or equal to 1:1[32,33] while for MDMO-PPV:PCBM blends the ratio is 1:4,[34] pointing to a much greater inherent miscibility between P3HT and PCBM. APFO-Green9:[70]PCBM blends present an optimum for a 1:3 ratio.

The physical properties of organic solvent used to dissolve the D−A blend dramatically affect the device performance. Several studies display an increase of PCE with the reduction of the solvent evaporation rate by using a high boiling point solvent.[35−37] However, contrary to P3HT, the use of such solvent with APFO-polymers does not help for the improvement of photovoltaic performances.

J_{sc} is correlated to the active layer morphology which is optimum when there is some small phase-separated domains (Figure 2c). J_{sc} is lower in the case of finer mixtures or in the case of bigger domains. Indeed, a very fine mixture does not allow a percolating path of the domains to the electrodes which is necessary for the charge transport and big domains act as traps for the charges decreasing the charge separation degree. A balance between both morphologies is then required.

It is tempting to suggest that the coarse morphology found with [70]PCBM is not impacting the photocurrent in a detrimental way. If we note the higher absorption generated by the C70 derivative (from EQE curves),[20] we may conclude that the exciton diffusion length is not much shorter than the critical dimension observed. We note that the domains observed in some blends (Figure 2c) is of the order of 100 nm, which would lead to photocurrent generation if the diffusion length of the exciton in the [70]PCBM phase would be ∼50 nm, a high but not impossible number.

5. General Discussion

Different parameters present a significant effect on the morphology of the active layer. The nature of substrate is one of these parameters. The observation of the active layer morphology on silicon substrate is not representative of the active layer morphology in the solar cells (on PEDOT:PSS-ITO) because of the surface energy difference.

The main parameters that determine the morphology of the blends are the D−A interactions and the solvent evaporation rate which can be tuned by the choice of the solvent.[38] For APFO-Green9:[70]PCBM blend, a high concentration of PCBM implies big domains while the use of DCB or a solvent mixture with DCB avoids the formation of domains. The morphology can then be modulated by the balance between these two parameters.

An active layer presenting small phase-separated domains seems to be the morphology that give the optimal performances. In the case of a APFO-Green9:[70]PCBM blend, this morphology is obtained with a 1:3 polymer:PCBM ratio and from chloroform solution. A previous study on the influence of solvent mixing on the morphology and performance of solar cells based on a blend of APFO3 and [60]PCBM[39] displays that the best performances of devices are obtained for a similar morphology with small domains. However, in this case, the active layer is spin-coated from chloroform:chlorobenzene (80:1) solvent mixture solution. It seems that whatever the nature of donor and acceptor materials, the nature of solvent, or solvent mixture, the morphology presenting phase-separated domains large enough to produce routes for charge transport, while a large interface for exciton dissociation is maintained, gives the optimal performance.

6. Conclusions

We investigated the influence of intrinsic (nature of the acceptor material) and extrinsic (concentration of the blend components, nature of the substrate and solvent) parameters on the nanoscale phase separation of APFO-Green9:[70]PCBM

blends. The morphological differences are explained by the relative miscibility between donor and acceptor materials, the solubility of the blend component depending on the solvent, and the wettability of the active layer onto the substrate. The best photovoltaic performances are obtained for the device presenting phase-separated domains which show a good balance between a large interfacial D−A area required for maximum exciton dissociation and continuous paths through both the D and A phases necessary for efficient charge transport between electrodes.

Acknowledgment. This research is supported by the Swedish Energy Agency and the Strategic Research Foundation SSF through the Center of Organic Electronics (COE).

References and Notes

(1) Peet, J.; Kim, J. Y.; Coates, N. E.; Ma, W. L.; Moses, D.; Heeger, A. J.; Bazan, G. C. *Nat. Mater.* **2007**, *6*, 497–500.
(2) Kim, J. Y.; Lee, K.; Coates, N. E.; Moses, D.; Nguyen, T. Q.; Dante, M.; Heeger, A. J. *Science* **2007**, *317*, 222–225.
(3) Park, S. H.; Roy, A.; Beaupré, S.; Cho, S.; Coates, N.; Moon, J. S.; Moses, D.; Leclerc, M.; Lee, K.; Heeger, A. J. *Nat. Photonics* **2009**, *3*, 297–303.
(4) Sariciftci, N. S.; Smilowitz, L.; Heeger, A. J.; Wudl, F. *Science* **1992**, *258*, 1474.
(5) Sariciftci, N. S.; Braun, D.; Zhang, C.; Srdanov, V. I.; Heeger, A. J.; Stucky, G.; Wudl, F. *Appl. Phys. Lett.* **1993**, *62*, 585.
(6) Yu, G.; Gao, J.; Hummelen, J. C.; Wudl, F.; Heeger, A. J. *Science* **1995**, *270*, 1789.
(7) Veldman, D.; Ipek, O.; Meskers, S. C. J.; Sweelssen, J.; Koetse, M. M.; Veenstra, S. C.; Kroon, J. M.; van Bavel, S. S.; Loos, J.; Janssen, R. A. J. *J. Am. Chem. Soc.* **2008**, *130*, 7721–7735.
(8) Hoppe, H.; Glatzel, T.; Niggemann, M.; Schwinger, W.; Schaeffler, F.; Hinsch, A.; Lux-Steiner, M. Ch.; Sariciftci, N. S. *Thin Solid Films* **2006**, *511−512*, 587–592.
(9) Jin, S. H.; Kumar Naidu, B. V.; Jeon, H. S.; Park, S. M.; Park, J. S.; Kim, S. C.; Lee, J. W.; Gal, Y. S. *Sol. Energy Mater. Sol. Cells* **2007**, *91*, 1187–1193.
(10) Barrau, S.; Heiser, T.; Richard, F.; Brochon, C.; Ngov, C.; Van de Wetering, K.; Hadziioannou, G.; Anokhin, D. V.; Ivanov, D. A. *Macromolecules* **2008**, *41*, 2701–2710.
(11) Economopoulos, S. P.; Chochos, C. L.; Gregoriou, V. G.; Kallitsis, J. K.; Barrau, S.; Hadziioannou, G. *Macromolecules* **2007**, *40*, 921–927.
(12) Thompson, B. C.; Fréchet, J. M. J. *Angew. Chem., Int. Ed.* **2008**, *47*, 58–77.
(13) Barrau, S.; Zhang, F.; Herland, A.; Mammo, W.; Andersson, M. R.; Inganas, O. *Appl. Phys. Lett.* **2008**, *93*, 023307.
(14) Zhang, F. L.; Jespersen, K. G.; Bjorstrom, C.; Svensson, M.; Andersson, M. R.; Sundstrom, V.; Magnusson, K.; Moons, E.; Yartsev, A.; Inganas, O. *Adv. Funct. Mater.* **2006**, *16*, 667–674.
(15) Chirvase, D.; Parisi, J.; Hummelen, J. C.; Dyakonov, V. *Nanotechnology* **2004**, *15*, 1317–1323.
(16) Roder, T.; Kitzerow, H. S.; Hummelen, J. C. *Synth. Met.* **2004**, *141*, 271–275.
(17) Wang, X. J.; Perzon, E.; Delgado, J. L.; De la Cruz, P.; Zhang, F.; Langa, F.; Andersson, M.; Inganas, O. *Appl. Phys. Lett.* **2004**, *85*, 5081–5083.
(18) Zhang, F.; Perzon, E.; Wang, X.; Mammo, W.; Andersson, M. R.; Inganas, O. *Adv. Funct. Mater.* **2005**, *15*, 745–750.
(19) Zhang, F.; Mammo, W.; Andersson, L. M.; Admassie, S.; Andersson, M. R.; Inganas, O. *Adv. Mater.* **2006**, *18*, 2169.
(20) Zhang, F.; Bijleveld, J.; Perzon, E.; Tvingstedt, K.; Barrau, S.; Inganas, O.; Andersson, M. R. *J. Mater. Chem.* **2008**, *18*, 5468–5474.
(21) Andersson, B. V.; Herland, A.; Masich, S.; Inganas, O. *Nano Lett.* **2009**, *9*, 853–855.
(22) Hoppe, H.; Niggemann, M.; Winder, C.; Kraut, J.; Hiesgen, R.; Hinsch, A.; Meissner, D.; Sariciftci, N. S. *Adv. Funct. Mater.* **2004**, *14*, 1005.
(23) Bjorstrom, C. M.; Bernasik, A.; Rysz, J.; Budkowski, A.; Nilsson, S.; Svensson, M.; Andersson, M. R.; Magnusson, K. O.; Moons, E. *J. Phys.: Condens. Matter* **2005**, *17*, L529–L534.
(24) Sehati, P.; Zhang, F.; Bijleveld, J.; Tvingstedt, K.; Andersson, M. R.; Inganas, O.; Fahlman, M. Private communication, **2007**.
(25) Bjorstrom, C. M.; Nilsson, S.; Bernasik, A.; Budkowski, A.; Andersson, M. R.; Magnusson, K. O.; Moons, E. *Appl. Surf. Sci.* **2007**, *253*, 3906–3912.
(26) Nilsson, S.; Bernasik, A.; Budkowski, A.; Moons, E. *Macromolecules* **2007**, *40*, 8291–8301.
(27) Arias, A. C.; MacKenzie, J. D.; Stevenson, R.; Halls, J. J. M.; Inbasekaran, M.; Woo, E. P.; Richards, D.; Friend, R. H. *Macromolecules* **2001**, *34*, 6005–6013.
(28) Bjorstrom, C. M.; Nilsson, S.; Magnusson, K. O.; Moons, E.; Bernasik, A.; Rysz, J.; Budkowski, A.; Zhang, F.; Inganas, O.; Andersson, M. R. *Proceedings of the SPIE Conference*, **2006**, Photonics Europe, Photonics Applications.
(29) Wienk, M. M.; Kroon, J. M.; Verhees, W. J. H.; Knol, J.; Hummelen, J. C.; van Hal, P. A.; Janssen, R. A. J. *Angew. Chem.* **2003**, *115*, 3493–3497.
(30) Yang, C. H.; Chang, J. Y.; Yeh, P. H.; Guo, T. F. *Carbon* **2007**, *45*, 2951–2956.
(31) Yao, Y.; Shi, C.; Li, G.; Shrotriya, V.; Pei, Q.; Yang, Y. *Appl. Phys. Lett.* **2006**, *89*, 153507.
(32) Li, G.; Shrotriya, V.; Huang, J.; Yao, Y.; Moriarty, T.; Emery, K.; Yang, Y. *Nat. Mater.* **2005**, *4*, 864–868.
(33) Reyes-Reyes, M.; Kim, K.; Dewald, J.; Lopez-Sandoval, R.; Avadhanula, A.; Curran, S.; Carroll, D. L. *Org. Lett.* **2005**, *7*, 5749–5752.
(34) Van Duren, J. K. J.; Yang, X.; Loos, J.; Bulle-Lieuwma, C. W. T.; Sieval, A. B.; Hummelen, J. C.; Janssen, R. A. J. *Adv. Funct. Mater.* **2004**, *14*, 425–434.
(35) Hoth, C. N.; Choulis, S. A.; Schilinsky, P.; Brabec, C. J. *Adv. Mater.* **2007**, *19*, 3973.
(36) Vanlaeke, P.; Vanhoyland, G.; Aernouts, T.; Cheyns, D.; Deibel, C.; Manca, J.; Heremans, P.; Poortmans, J. *Thin Solid Films* **2006**, *511*, 358.
(37) Chen, F. C.; Tseng, H. C.; Ko, C. J. *Appl. Phys. Lett.* **2008**, *92*, 103316.
(38) Nilsson, S.; Bernasik, A.; Budkowski, A.; Moons, E. *Macromolecules* **2007**, *40*, 8291–8301.
(39) Zhang, F.; Jespersen, K. G.; Bjorstrom, C.; Svensson, M.; Andersson, M. R.; Sundstrom, V.; Magnusson, K.; Moons, E.; Yartsev, A.; Inganas, O. *Adv. Funct. Mater.* **2006**, *16*, 667–674.